J Mater Sci (2012) 47:7003–7012
DOI 10.1007/s10853-012-6651-4

Poly(methyl methacrylate)–TiO_2 nanocomposites obtained by non-hydrolytic sol–gel synthesis: the innovative *tert*-butyl alcohol route

D. Morselli · F. Bondioli · M. Fiorini · M. Messori

Received: 19 April 2012 / Accepted: 8 June 2012 / Published online: 26 June 2012

Abstract The present article concerns the preparation of poly(methyl methacrylate)/titania nanocomposites by a non-conventional bottom-up approach, as alternative to the conventional mechanical compounding of preformed filler particles. Poly(methyl methacrylate) (PMMA) was modified with in situ generation of titania nanoparticles by means of the so-called non-hydrolytic sol–gel (NHSG) process in the presence of *tert*-butyl alcohol (*t*BuOH) as oxygen donor and polymer solvent. The results showed that the synthetic procedure used permitted the preparation of the highly filled PMMA (up to 20 phr of titania in anatase form) with titania actual content values very close to the nominal ones and with enhanced filler dispersion and homogeneous distribution within the polymeric matrix, avoiding the typical rheological problems related to distributive and dispersive mixing of conventional compounding methods. The presence of titania nanoparticles led to increases in glass transition temperature and E' modulus in the rubbery region for all the prepared samples with respect to the pristine PMMA. Finally, the nanocomposites showed an interesting photo-catalytic activity towards organic molecules. The findings led us to conclude that the NHSG process was successfully employed to produce anatase titania in the presence of *t*BuOH and PMMA. The proposed process seems to offer a very promising method to produce polymer nanocomposites with good filler dispersion and homogeneous distribution and with interesting functional properties such as photo-catalytic activity.

D. Morselli · F. Bondioli · M. Messori (✉)
Dipartimento di Ingegneria dei Materiali e dell'Ambiente, Università di Modena e Reggio Emilia, Via Vignolese 905/A, 41125 Modena, Italy
e-mail: massimo.messori@unimore.it

M. Fiorini
Dipartimento di Ingegneria Civile, Ambientale e dei Materiali, Università di Bologna, Via Terracini 28, 41131 Bologna, Italy

Introduction

Nanoscience and nanotechnology researches have been drawing a considerable attention in materials science, since the last decade. The development of nanocomposite materials, based on inorganic filler embedded in organic matrix, such as a polymer, is particularly interesting in this field. The incorporation of inorganic nanoparticles, such as ceramic oxides, into a polymer matrix leads to materials with enhanced properties as compared with both unfilled polymers and polymers filled with micrometric particles. Moreover, the presence of filler is able to change deeply the thermo-mechanical, optical, electrical, and magnetic properties of a polymeric matrix. Obviously, these properties are strongly dependent on the nature of the constituents, but also on shape, size distribution and crystallinity of the incorporated particles [1–3]. Furthermore, the use of nano, instead of microfillers, allows obtaining materials characterized by as good properties as microcomposites but having lower filler content, which is due to the much higher interfacial area between the filler and the matrix [4].

In bibliography, there are many articles about polymeric nanocomposites filled with ceramic oxides, nanoparticles, and a wide range of synthesis methods are described for developing this new interesting type of materials [5–9]. However, in order to prepare nanocomposites, the so-called top-down approach, where ex situ-preformed nanoparticles have to be dispersed into the polymeric matrix by physical–mechanical mixing, is still widely used [10, 11]. Although the method just described is still attractive from an

industrial point of view, it presents some severe limitations related to the difficulties to obtain an effective filler dispersion and a homogenous distribution due to the strong tendency of the nanoparticles to agglomerate and the significant increase of the viscosity because of the complex system rheology [12]. An alternative and innovative technique, for overcoming the complications above described, is the bottom-up approach that concerns an in situ generation of filler (generally metal oxides) by a chemical reaction [12]. Employing this route, the filler grows up directly into the polymeric matrix without the need for further steps. The sol–gel reaction is one of the most useful and simple ways employed towards this target.

The sol–gel process is a chemical technique, initially employed to prepare high-purity inorganic networks such as glasses and ceramic materials. Mild conditions characterize this method, which becomes a strategic point when organic materials are involved into the process, permitting to avoid their thermal degradation. Typical precursors are metal (or non metal) alkoxides which, reacting with water in the presence of an adequate basic catalyst, lead to nanoparticles having narrow grain size distribution with average dimensions between 5 and 100 nm.

The so-called hydrolytic (or aqueous) sol–gel reaction is generally divided into two steps: the first one named hydrolysis where hydroxyl groups are produced, and the second one named condensation, where the polycondensation of hydroxyl groups and/or residual alkoxyl groups [13, 14] are involved to form a three-dimensional (3D) network, according to the following scheme:

$$\text{Hydrolysis} \quad \mathrm{M(OR)}_x + n\mathrm{H_2O} \rightarrow \mathrm{M(OR)}_{x-n}\mathrm{OH}_n + n\mathrm{ROH}$$

$$\text{Condensation} \quad \equiv\mathrm{M-OH} + \mathrm{HO-M}\equiv \rightarrow \equiv\mathrm{M-O-M}\equiv + \mathrm{H_2O} \ \text{(by water elimination)}$$

$$\text{and/or} \quad \equiv\mathrm{M-OR} + \mathrm{HO-M}\equiv \rightarrow \equiv\mathrm{M-O-M}\equiv + \mathrm{ROH} \ \text{(by alcohol elimination)}$$

The presence, in the reaction medium, of an organic oligomer or polymer leads to the formation of organic–inorganic hybrid structures composed of inorganic oxide and organic matrix intimately mixed each other [15, 16]. The optical, physical and mechanical properties of nanocomposites depend strongly not only on the individual properties of each component, but also on filler phase constituents, domains size and the molecular mixing at the phase boundaries, all characteristics that the sol–gel method permits to achieve under strict control. In spite of these advantages, it is necessary to underline that the crystallinity of the inorganic phase so obtained is generally quite low. For this reason, during the last 20 years, a lot of researches have been performed about the non-hydrolytic (or non-aqueous) sol–gel (NHSG) reaction, to obtain very pure and crystalline inorganic oxides, such as silica [17], V_2O_3, Nb_2O_5, SnO_2, In_2O_3, HfO_2, Ta_2O_5, Ga_2O_3, ZnO, Y_2O_3 and γ-Fe_2O_3/Fe_3O_4, etc. [18–23].

The NHSG process, as well as the aqueous route, is split in two reaction steps. In the first step, either a metal (or non-metal) halide or alkoxide reacts with an organic oxygen donor (such as alcohols, ether, etc.). The second step, named condensation, can follow different pathways. The most common reactions are those between an organic alcohol and a metal (or non-metal) halide, which usually lead to a condensation through alkyl halide elimination and/or ether elimination pathways [24–28] and are listed as follows:

$$\text{Alcoholysis} \quad \mathrm{MX}_m + n\mathrm{ROH} \rightarrow \mathrm{M(X)}_{m-n}(\mathrm{OR})_n + n\mathrm{HX}$$

$$\text{Condensation} \quad \equiv\mathrm{M-OR} + \mathrm{RO-M}\equiv \rightarrow \equiv\mathrm{M-O-M}\equiv + \mathrm{R-O-R} \ \text{(by ether elimination)}$$

$$\text{and/or} \quad \equiv\mathrm{M-OR} + \mathrm{X-M}\equiv \rightarrow \equiv\mathrm{M-O-M}\equiv + \mathrm{R-X} \ \text{(by alkyl-halide elimination)}$$

Regarding titanium dioxide, several articles have reported the reaction between titanium tetrachloride and benzyl alcohol [29–32] to obtain pure titanium dioxide crystallized in anatase phase that would not have materialized when employing the hydrolytic method which is characterized by the obtainment of an amorphous phase [33].

The aim of the present study was to prepare PMMA/TiO_2 nanocomposites by the formation of organic–inorganic hybrid structures applying an innovative synthesis method based on NHSG process. The NHSG reaction was employed for the in situ generated filler to overcome the typical problems related to the hydrolytic way, in which the low miscibility of the sol–gel aqueous system strongly limits the dispersion and distribution of the filler within the polymeric matrix. The authors [34, 35] already reported the use of this innovative approach to prepare epoxy resin/titania and PMMA/titania nanocomposites. In both cases, independent of the chosen polymer matrix, improvements in the mechanical and functional properties were observed, thanks to the high interfacial interactions between organic and inorganic phases as a result of the bottom-up approach.

Regarding the PMMA/titania composite, in this study, a new route has been proposed using *tert*-butyl alcohol (*t*BuOH) as oxygen donor that allowed employing mild condition during solvent elimination step having a lower boiling point than benzyl alcohol (82 and 206 °C, respectively). This aspect becomes strategically important when a sol–gel reaction is employed in the preparation of composites based on polymeric matrix, permitting a complete solvent evaporation using milder conditions to avoid the polymer chains degradation and/or plasticizing effects. Moreover, *t*BuOH is not only the reaction oxygen donor but,

Table 1 Sample codes and concerning descriptions

Sample code	Sample description
T70	TiO_2 synthesized by NHSG at 70 °C
PMMA_0T	PMMA solved in *t*BuOH and dried by rotary evaporator
PMMA_5T	PMMA/TiO_2 composite prepared by in situ generation of TiO_2 (nominal content 5 phr) at 70 °C
PMMA_15T	PMMA/TiO_2 composite prepared by in situ generation of TiO_2 (nominal content 15 phr) at 70 °C
PMMA_20T	PMMA/TiO_2 composite prepared by in situ generation of TiO_2 (nominal content 20 phr) at 70 °C

thanks to alkyl group steric effect, it can also act as capping agent and, thus, as particles size and phase controller.

In order to study the effect of the inorganic phase on the polymeric matrix, the microstructure, the thermo-mechanical properties and photo-activity of the obtained materials were evaluated.

Experimental

Chemicals

Titanium (IV) tetrachloride ($TiCl_4$), *t*BuOH and methylene blue (MB) were purchased from Sigma Aldrich (Milan, Italy). Poly(methyl methacrylate) (PMMA, Optixâ CA-1000 I Clear) commercial grade was supplied by Plaskolite West Inc., CA (melt flow rate 2.3 g/10 min at 230 °C/3.8 kg). All the chemicals were used as received without further purification.

Materials preparation

PMMA/TiO_2 nanocomposites were prepared by NHSG process with three nominal titania contents, respectively: 5, 15, and 20 phr (parts per hundred resin). A typical preparation was as follows: about 2 g of PMMA was dissolved in 100 ml of *t*BuOH at 70 °C. After the dissolution, the correct amount of $TiCl_4$ (0.15, 0.43, and 0.58 ml, respectively) was added dropwise at room temperature under vigorous stirring. The reaction was kept under stirring at room temperature for 15 min and then warmed up to 70 °C for 24 h.

The whitish suspensions obtained were partially dried (about 50 % of the initial volume) by rotary evaporator at 40 °C under vacuum. In order to completely eliminate the residual *t*BuOH and other volatiles, the remaining suspensions were cast in a mould and maintained under an aspiration hood overnight. Finally, the specimens were placed in an electric oven at 75 °C under vacuum for 5 h.

To better characterize the inorganic phase, titanium dioxide was also synthesized under the same conditions without any amount of PMMA. A list of the prepared samples and their descriptions are reported in Table 1.

TiO_2 powders characterization

The synthesized titania was analysed by a computer-assisted conventional Bragg–Brentano diffractometer (PW3710 Philips) using the Ni-filtered CuK_α monochromatic radiation ($\lambda = 1.5418$ Å) to identify the crystalline phase. The X-ray diffraction (XRD) patterns were collected at room temperature in 10–60° 2θ range, with a scanning rate of 0.005°/s and a step size of 0.02°.

Quantitative analysis of T70 was performed by the combined Rietveld-RIR (Reference Intensity Ratio) method. A 10 wt% of corundum (NIST SRM 674a annealed at 1500 °C for 1 day to increase crystallinity to 100 wt%) was added to the sample as internal standard. The mixture, ground in an agate mortar, was side-loaded in an aluminium flat holder to minimize the preferred orientation problems. Data were recorded in the 2θ range of 5–140° (step interval 0.02° and 6 s counting time for each step). The phase fractions extracted by the Rietveld-RIR refinements, using GSAS and EXPGUI [36, 37], were rescaled on the basis of the absolute weight of the corundum originally added to the mixture as an internal standard, and therefore internally renormalized.

The amount of volatile fraction on the particles surface was evaluated by thermogravimetric/differential thermal analysis (TG–DTA, Netzsch STA 429 CD) for measuring the percentage of weight loss as a function of temperature. The measurement was carried out in the temperature range between 25 and 700 °C, using 20 °C min^{-1} as heating rate.

In order to investigate the presence of residual organic groups and/or free OH on the sample surface an FT-IR analysis was performed on the obtained powder. The analysis was carried out using an FTIR Vertex 70 spectrometer (Bruker) in ATR mode, equipped with a diamond crystal.

Particles morphology was examined by transmission electron microscopy (TEM), (JEM 2010, Jeol, Japan). A drop of the obtained suspension was placed on a copper grid covered with a transparent polymer, followed by drying.

The specific surface area (SSA) and the density of the powders were determined by the BET method [38] (Gemini 2360 apparatus, Micromeritics, Norcross, GA, USA) and by a picnometer (Accupic 1330 apparatus, Micromeritics,

Norcross, GA, USA), respectively. The particles size was also calculated from Eq. 1, using SSA and density data previously carefully measured:

$$\Phi = \frac{6}{(S \cdot \rho)} \quad (1)$$

where Φ is the average diameter of the spherical particle, S and ρ are, respectively the experimental SSA and the experimental real density of the obtained powders [39].

The photo-catalytic activity of the synthesized powders was evaluated by MB dye decomposition. About 0.01 g of TiO_2 powder was dispersed in 75 ml of 3×10^{-5} M MB aqueous solution. The suspension was kept under stirring (by magnetic stirrer) in a dark chamber for 24 h under UV irradiation. The UV lamp employed had the wavelength ranging between 300 and 450 nm, and the light intensity was 5.5 mW cm^{-2} on the liquid surface (Hamamatsu Lightningcure LC8, 365 type). The MB solution concentration was monitored at regular intervals by UV–Vis spectrophotometer (Perkin-Elmer, Lambda 19) in the range of 500–700 nm for evaluating the absorbance variation at 664 nm. Calibration, based on Lambert–Beer law, was used to quantify the dye concentration.

The photo-degradation of MB was calculated by Eq. 2:

$$\text{Photo-degradation} = \frac{(C_0 - C_t)}{C_0} \quad (2)$$

where C_0 is the MB concentration at $t = 0$ min and C_t is the MB concentration at the generic time t considered.

PMMA/TiO_2 composites characterization.

The effective titania content in the composites was evaluated by gravimetric analysis. The sample weight was determined before and after the organic matrix combustion in an electric furnace (Optolab—FS5) at 500 °C.

The thermal stability of prepared composites was evaluated by thermogravimetric analysis (TGA, Perkin–Elmer TGA7 Thermogravimetric Analyzer) for measuring the percentage of weight loss as a function of temperature. The measurement was carried out under nitrogen flow and in the temperature range between 30 and 600 °C, using 10 °C min^{-1} as heating rate.

Composite's microstructure was investigated by field emission scanning electron microscopy (FESEM, Carl Zeiss—Supra 40) by applying a gold-coating (about 5 nm) over the fractured surfaces (by liquid nitrogen).

The polymer molecular weight was measured by gel permeation chromatography (GPC) using chloroform as eluent (elution rate of 0.3 ml/min) on a HPLC Pump (Waters 1515) equipped with a refractive index detector (Waters 2410) and a PL gel Mixed-D column.

The glass transition temperature (T_g), storage modulus (E') and loss factor (tanδ) were determined through dynamic-mechanical thermal analysis (DMTA). The characterisation was performed by means of a dynamic-mechanical thermal analyser (Rheometric Scientific DMTA 3E) equipped with a single cantilever bending frame geometry. First, to evaluate the limits of linear viscoelastic, a strain sweep test (at 25 °C) was performed on neat PMMA (specimen dimension $22 \times 6 \times 2$ mm^3). All the samples were analysed at temperatures ranging from −50 to 160 °C with a heating rate of 3 °C min^{-1}, an oscillatory frequency of 1 Hz and a deformation of 0.025 %, the values well within the linear viscoelastic range for all composites. The specimens were prepared by injection moulding using a Minimax Moulder (Custom Scientific Instruments) at 280 °C.

Differential scanning calorimetry (DSC) was carried out on a Thermal Analysis TA2010 Instruments at a heating rate of 10 °C min^{-1} at temperatures ranging from −10 to 200 °C. The glass transition temperature was assumed as the mean value of the energy jump of the thermogram (average value between the onset and the endpoint of the glass transition range).

In order to evaluate if the photo-catalytic activity of the powder was maintained even in the nanocomposites, the MB decomposition (calculated by Eq. 2) was determined using the same method, and same conditions were employed for the powder characterization. The specimens (dimension $22 \times 6 \times 2$ mm^3) were dipped in a beaker containing 75 ml of 3×10^{-5} M aqueous solution of MB. The solutions were kept under magnetic stirring in a dark chamber for 24 h under an UV irradiation.

Results and discussion

TiO_2 powders characterization

T70 XRD pattern is reported in Fig. 1, which shows that the powder is composed by anatase (JCPDS file 01-075-1537) as crystalline phase, whereas the broadened peaks are a common characteristic when the powder has nanometric sizes.

To quantify the amorphous phase in the synthesized powders, Rietveld-RIR analysis was performed (values reported in Table 2). The NHSG synthesis led to powders with higher crystallization degree (almost 23 wt%) in comparison to the completely amorphous powders synthesized by aqueous sol–gel method as reported elsewhere [40]. When compared with the data reported by Messori et al. [35] relating to titania powders obtained by NHSG by using the benzyl alcohol route, the obtained crystallinity is slightly lower (23 instead of almost 39 wt%) than the powders obtained at the same temperature of 70 °C.

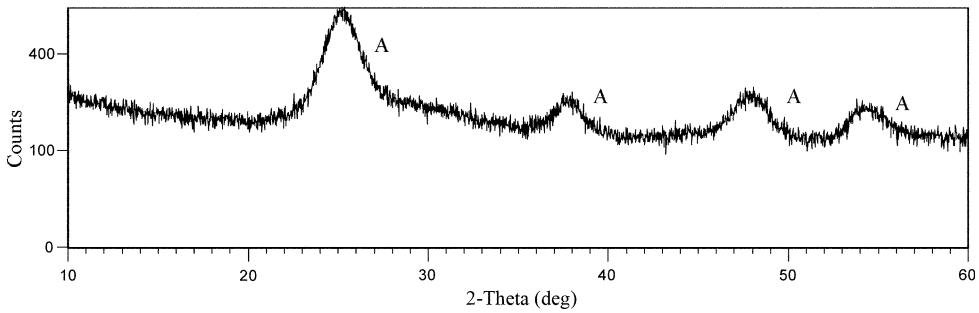

Fig. 1 XRD pattern of powder (T70) synthesized by means of NHSG process (*A*, anatase peaks)

Table 2 Properties of the T70 powder: SSA, density, average diameter (Φ, by Eq. 1) and quantitative Rietveld-RIR analysis results and standard Rietveld agreement factors (χ^2, R_{wp}, R_p)

Sample code	SSA (m^2 g^{-1})	Density (g cm^{-3})	Φ (nm) by Eq. 1	Amorphous (wt%)	Anatase (wt%)	χ^2	R_{wp} (%)	R_p (%)
T70	86.8 ± 1.7	2.606 ± 0.002	26.5 ± 0.6	77.4 ± 0.1	22.6 ± 0.1	1.800	0.0466	0.0339

The measured physical properties of the powder are reported in Table 2. The SSA was about 85 m^2 g^{-1}; this value is rather high, as expected, considering the nano size of the grains. The real density of the powder is 2.60 g cm^{-3}, lower than the value in the literature that is around 3.90 g cm^{-3} for pure anatase, and about 4 g cm^{-3} for rutile and brookite [41]. This difference may be due to the large amount of amorphous phase (more than 70 %) that strongly affected the density value. This aspect was also confirmed by TG–DTA curve (Fig. 2), which presents two main weight losses. In particular, the endothermic peak at 100 °C, correlated to 6 % of weight loss, was attributed to the desorption of the physical adsorbed water. The second and third exothermic peaks are rather overlapped, and they were correlated to the weight loss of 7 %, between 200 and 550 °C. This can be tentatively explained by attributing the weight loss, in this temperature range, to the hydroxyl group condensation associated with anatase crystallization, the behaviour already observed by Bondioli et al. [33].

FT-IR spectrum reported in Fig. 3 shows a broad band centred at 3,100 cm^{-1} that is typically due to the free O–H stretching [42] bonds, which result is in good agreement with both the second weight loss observed in TG–DTA analysis and the presence of amorphous phase evaluated by quantitative XRD analysis. The peak found at 1,630 cm^{-1} was attributed [42] to the presence of the adsorbed water as confirmed in TG curve by the weight loss at 100 °C.

Figure 4 reports the TEM image of the obtained titania particles. The micrograph shows nanometric spherical crystals in the range of 5–10 nm tightly connected to create small agglomerates.

T70 average particles size was also calculated employing SSA and density values following Eq. 1 (Table 2), assuming that the particles are closed spheres with smooth surfaces (which is a reasonable hypothesis, as supported by TEM). The slight difference between the average particle size as measured by TEM (8 nm) and as calculated by Eq. 1 (26 nm) suggests the presence of a limited agglomeration phenomena.

The photo-catalytic activity of the obtained powder was determined studying the degradation of MB taking into account also its non-catalysed degradation only due to the UV light. The MB photo-degradation, as a function of UV irradiation time, was evaluated (by Eq. 2) both without any catalyst and in the presence of T70 dispersed in the dye solution. The curves are reported in Fig. 5 where a

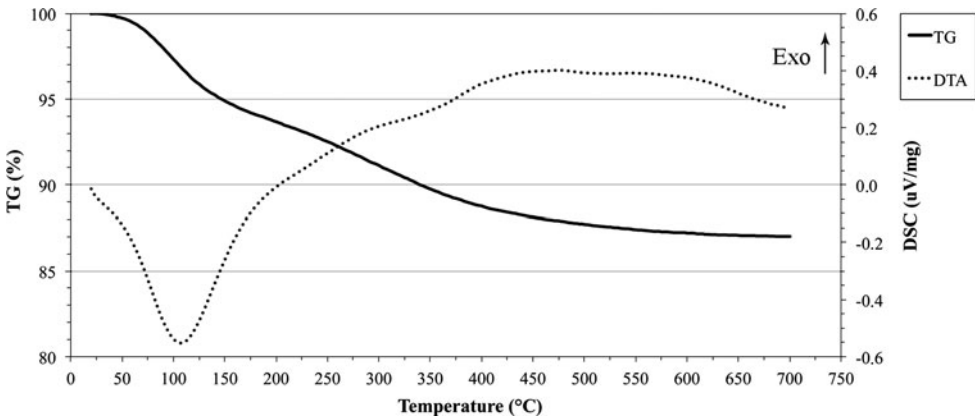

Fig. 2 Thermal gravimetric analysis of the powder (T70) synthesized by means of NHSG process

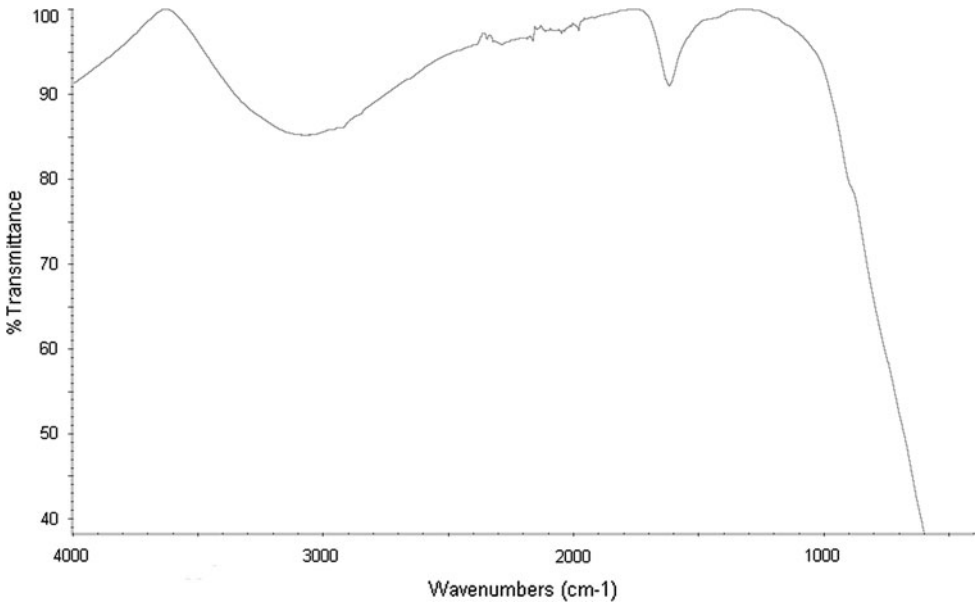

Fig. 3 FT-IR spectrum of powder (T70) synthesized by means of NHSG process

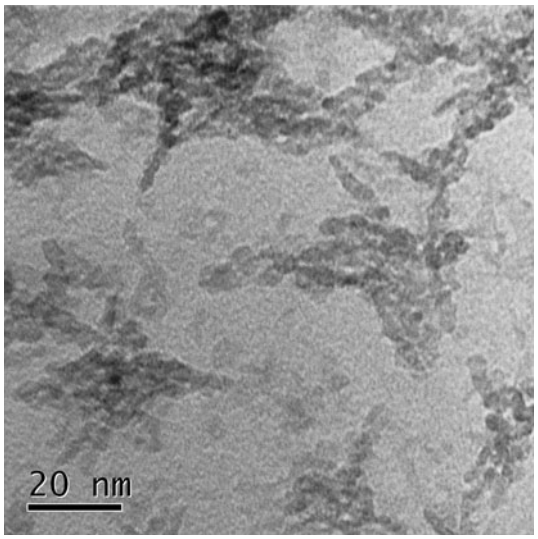

Fig. 4 TEM micrography of titania nanoparticles (T70) synthesized by means of NHSG process

significant catalytic activity of titania is clearly shown. T70 was able to promote, when irradiated by UV light, an almost complete MB photo-degradation (0.90) in about 15 h, whereas, in non-catalysed condition, the photo-degradation of MB at 24 h was lower than 0.40.

PMMA/TiO_2 composites' characterization

The FESEM micrographs of the fracture surfaces of PMMA_5T and PMMA_20T composites are reported in Fig. 6a–c. A slightly rough fracture surface was present in both the investigated samples, and the same matrix morphology was also observed for neat PMMA_0T (micrograph here not reported). Morphology characterized by the presence of very well-distributed particles having a spherical shape with maximum diameter <100 nm was observed for all specimens. The chemical compositions of the particles were consistent with the expected titania as indicated by energy dispersive X-ray spectrometry (EDS, here not reported). FE-SEM analysis indicated that the NHSG method was an effective process to obtain nanocomposite materials with good dispersion and homogeneous distribution of nanoparticles avoiding significant agglomeration of particles.

The composite actual filler content was evaluated for each sample by thermo-gravimetric analysis, and the final results are reported in Table 3. The actual titania contents, in situ generated, were significantly close to the expected values. This suggests that the sol–gel reaction yields amounted to about 100 % for all samples and, therefore, that the conversion of $TiCl_4$ was not affected by the presence of PMMA in the reaction medium. This aspect represents a significant improvement with respect to the previously reported data on similar systems obtained by means of benzyl alcohol [35] instead of *t*BuOH. In that case, the necessity of precipitation, filtration and washing steps for the elimination of high boiling point benzyl alcohol led to a significant reduction of the actual titania content compared with the nominal one.

In addition, as shown by the TG curves reported in Fig. 7, the TiO_2 nanoparticles did not change significantly the PMMA thermal stability. This represents a further positive result considering that the presence of the in situ-generated titania often causes a strong decrease in thermal stability as per the recently published result for epoxy resin/titania composites prepared by aqueous sol–gel process [43].

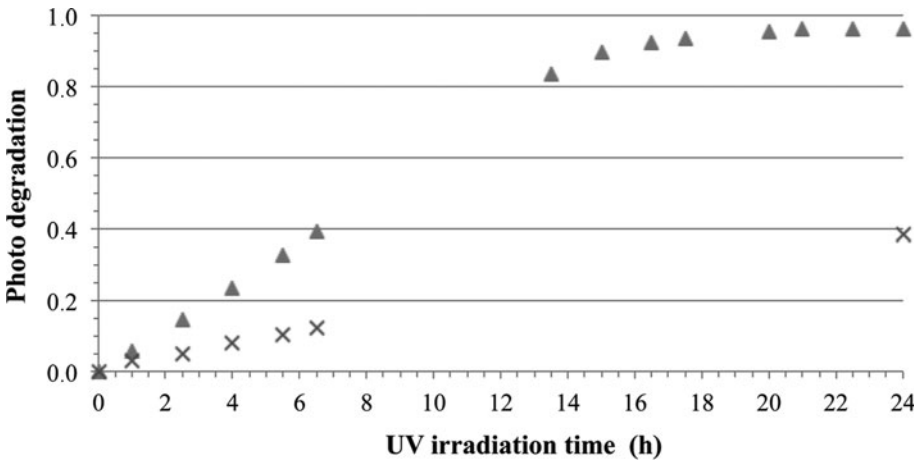

Fig. 5 MB photo-degradation (*times*) and catalysed by T70 (*filled triangle*) (calculated using Eq. 2) as a function of UV irradiation time

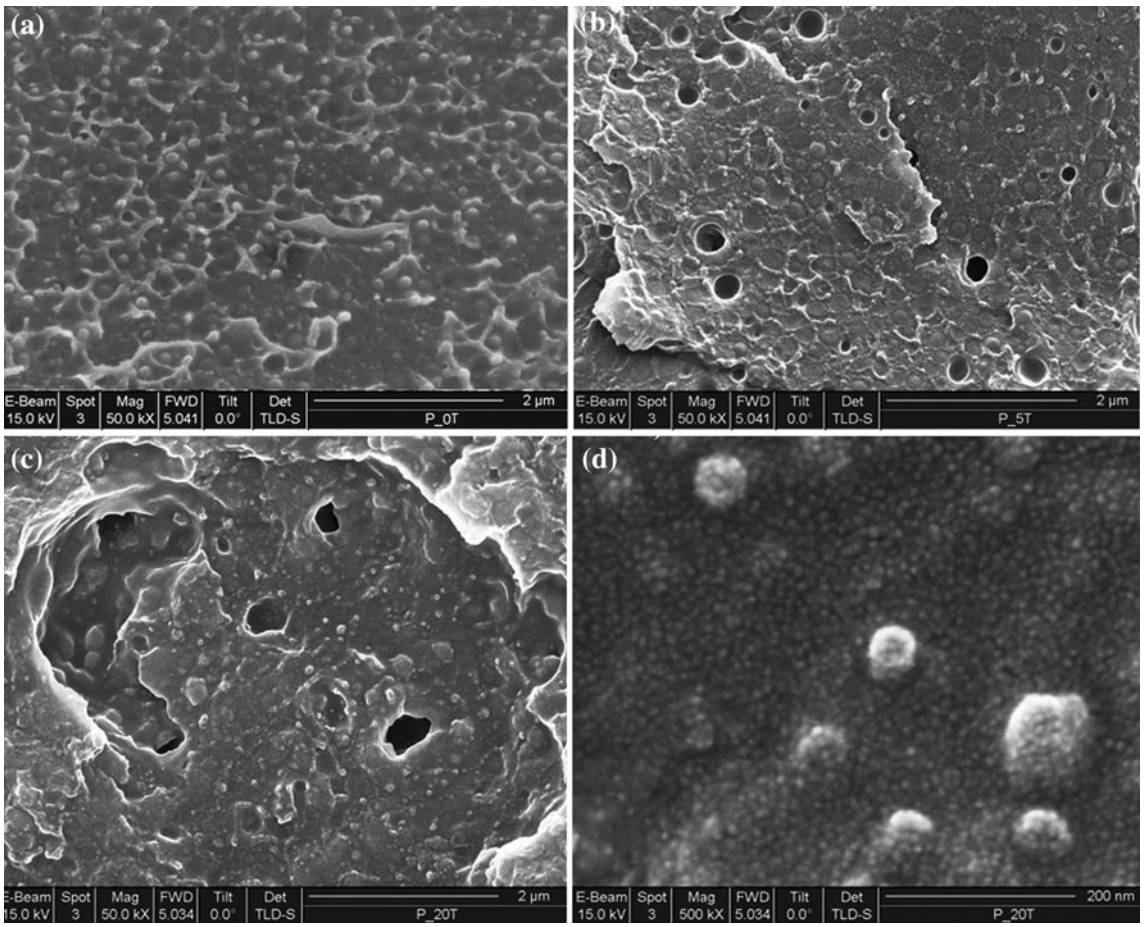

Fig. 6 FESEM micrographies of fracture surface of PMMA_0T (**a**), PMMA_5T (**b**) and PMMA_20T (**c**, **d**)

In order to evaluate possible degradation effects on the polymer during the sol–gel reaction, due to the evolution of aggressive chemicals such as hydrochloric acid and other by-products, the molecular weight and molecular weight distribution were evaluated by GPC. GPC traces (here not reported) showed a complete overlapping for all samples. This aspect indicates that the in situ generation of titania from $TiCl_4$ did not affect the polymer molecular weight and molecular weight distribution demonstrating the absence of significant degradation reactions during the filler synthesis.

The values of E' measured in the rubbery region (in a temperature range between 170 and 185 °C, that is about $T_g + 50$ °C), damping (expressed as maximum value of loss factor, $\tan\delta_{max}$) and of glass transition temperature

Table 3 Properties of PMMA/TiO_2 composites: nominal and actual TiO_2 content, glass transition temperature (T_g) by DMTA and DSC, storage modulus measured at $T = T_g + 50$ °C (E'_{T_g+50}), damping (expressed as maximum value of tanδ, tanδ_{max}) and photo-degradation rate at 24 h

Sample code	Nominal TiO_2 content (phr)	Actual TiO_2 content (phr)	T_g (°C) by DMTA	T_g (°C) by DSC	E'_{T_g+50} (MPa)	tanδ_{max} (–)	Photo-degradation rate at 24 h (–)
PMMA_0T	–	–	121	102	1.46	1.30	0.49
PMMA_5T	5	5.0	127	113	1.78	1.12	0.59
PMMA_15T	15	14.9	132	115	2.45	0.93	0.71
PMMA_20T	20	20.6	134	119	4.23	0.79	0.72

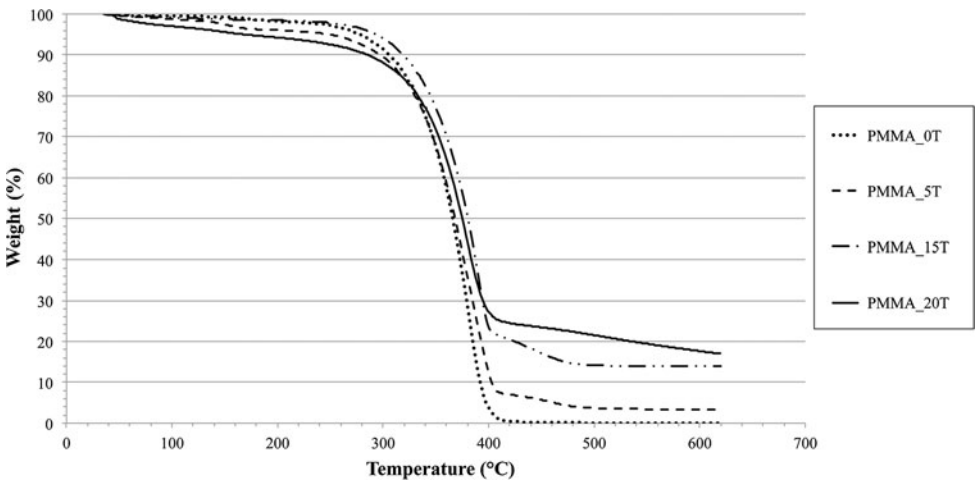

Fig. 7 TGA of PMMA/TiO_2 composites

(determined as peak value of loss factor tanδ) are reported in Table 3. All properties, just described, were changed by the presence of TiO_2 nanoparticles. As expected, a remarkable reduction of damping and an increment of T_g were found when the titania content increased. T_g values increased from 121 °C for unfilled PMMA (PMMA_0T) to about 127, 132 and 134 °C for PMMA_5T, PMMA_15T and PMMA_20T, respectively, evidencing a typical constrain of mobility chains effect due to the presence of rigid fillers within the polymeric matrix (Fig. 8a). These results are in good agreement with DSC data (reported in Table 3), which confirmed the same T_g trend. Concerning the E' modulus, it was not significantly affected in the glassy region, whereas an interesting trend was found in the rubbery region (values of E'_{T_g+50} are reported in Table 3). E'_{T_g+50} of PMMA_0T (about 1.46 MPa) increased up to 1.78, 2.45 and 4.23 MPa for PMMA_5T, PMMA_15T and PMMA_20T, respectively. In Fig. 8b, the E' modulus is reported as a function of temperature, which showed clearly that, in the rubbery region, the stiffening effect increases with the titania content.

Finally, the specimens' photo-catalytic activity was determined by the degradation of MB taking into account the dye's auto-degradation only due to the UV light. All degradation kinetic curves obtained are reported in Fig. 9. The reaction rate in the first 8 h did not present substantial differences, whereas after 24 h the samples (values reported in Table 3) showed significant MB degradation. PMMA_0T led to a photo-degradation, after 24 h, slightly higher than MB auto-degradation (0.48 and 0.39, respectively). The photo-degradation values at 24 h for PMMA_5T, PMMA_15T and PMMA_20T increased to 0.59, 0.71 and 0.72, respectively. These results suggested that titania, on the specimen's surfaces, maintains its photo-catalytic activity even when it is embedded in a polymer matrix. PMMA_15T and PMMA_20T presented the highest photo-degradation. The values are, however, very similar, probably related to TiO_2 particles size which increases with the filler content, leading to a lower surface area causing a decrease of expected trend.

Conclusions

Titania nanoparticles of average size of 5–10 nm partially in anatase form were in situ generated within PMMA by means of NHSG process. The particles were uniformly distributed and well dispersed without significant particle–particle aggregation thanks to the bottom-up approach used for the synthesis. The actual content of titania was very close to the nominal one indicating the effectiveness of the synthesis and solvent elimination procedures. The in situ generation of titania did not lead to any negative effect on the PMMA molecular weight and thermal stability. On the contrary, a significant stiffening effect (increase of both T_g

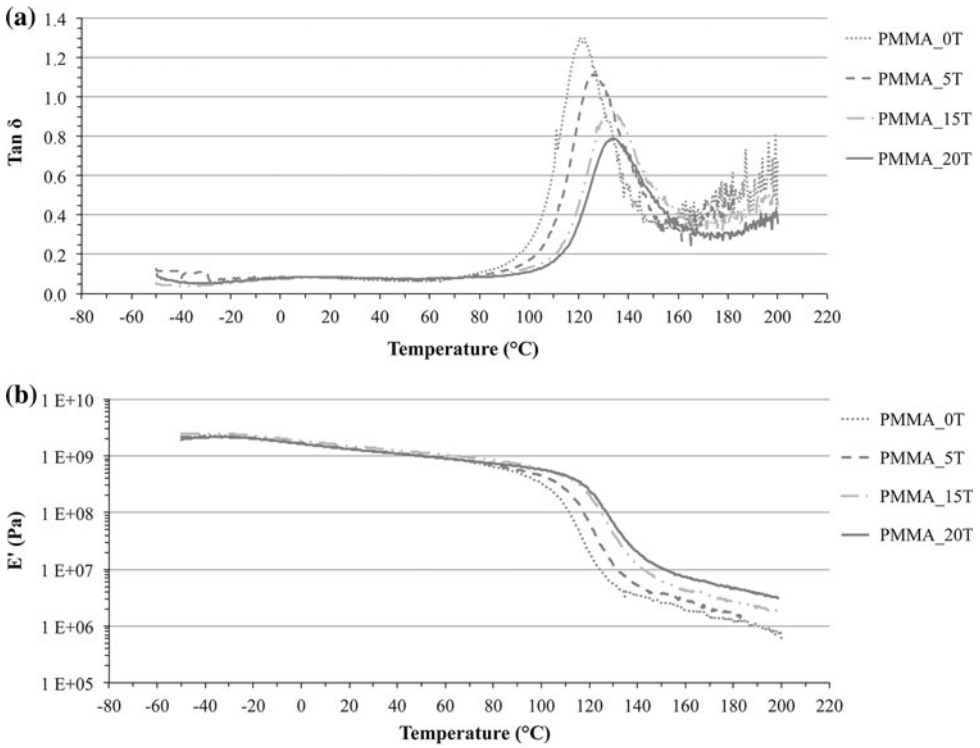

Fig. 8 Loss factor (tanδ, '**a**') and storage modulus (E', '**b**') as a function of temperature

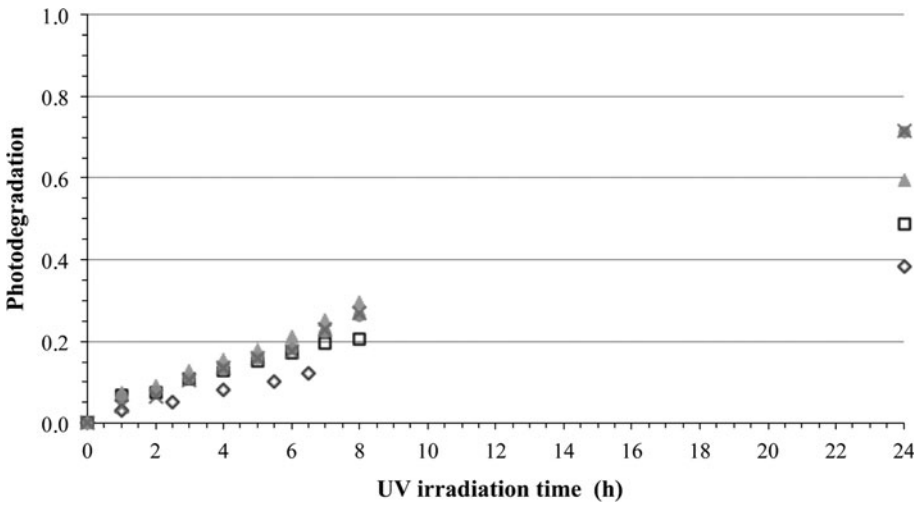

Fig. 9 MB degradation catalysed by nanocomposites (calculated by Eq. 2) as a function of UV irradiation time. *Open diamond* photo-degradation, *open square* PMMA_0T, *filled triangle* PMMA_5T, *filled circle* PMMA_15T, *times* PMMA_20T

and storage modulus) was observed in the case of filled PMMA. Photo-degradation tests showed that the presence of anatase produced a significant photo-catalytic activity of the PMMA-based composites, which can in principle be used for applications in the fields of water purification and self-cleaning surfaces.

References

1. Ajayan PM, Schadler LS, Braun PV (2003) Nanocomposite science and technology. Wiley-VCH, Weinheim
2. Liu TB, Burger C, Chu B (2003) Prog Polym Sci 28(1):5
3. Kickelbick G (2003) Prog Polym Sci 28(1):83
4. Schmidt G, Malwitz MM (2003) Curr Opin Colloid Interface Sci 8(1):103. doi:10.1016/s1359-0294(03)00008-6
5. Hamming LM, Qiao R, Messersmith PB, Brinson LC (2009) Compos Sci Technol 69(11–12):1880. doi:10.1016/j.compscitech.2009.04.005
6. Matsuyama K, Mishima K (2007) J Supercrit Fluid 40(1):117. doi:10.1016/j.supflu.2006.04.002
7. Bressy C, Ngo VG, Leroux C, Margaillan A (2009) Polymer 50(14):3095. doi:10.1016/j.polymer.2009.04.077
8. Jeremic K, Dzunuzovic E, Nedeljkovic JM (2007) Eur Polym J 43(9):3719. doi:10.1016/j.eurpolymj.2007.06.026
9. Convertino A, Leo G, Tamborra M, Sciancalepore C, Striccoli M, Curri ML, Agostiano A (2007) Sensors Actuators B 126(1):138. doi:10.1016/j.snb.2006.11.043
10. Bondioli F, Cannillo V, Fabbri E, Messori M (2005) J Appl Polym Sci 97(6):2382

11. Bondioli F, Dorigato A, Fabbri P, Messori M, Pegoretti A (2009) J Appl Polym Sci 112(2):1045. doi:10.1002/App.29472
12. Messori M (2011) In: Recent advances in elastomeric nanocomposites. advanced structured materials, vol 9. Springer/GmbH & Co. K, Berlin, pp 57–88. doi:10.1007/978-3-642-15787-5_2
13. Brinker CJ, Scherer GW (1990) Sol-gel science: the physics and chemistry of sol–gel processing. Academic Press, Boston
14. Wen JY, Wilkes GL (1996) Chem Mater 8(8):1667
15. Messori M, Fiorini M (2011) J Appl Polym Sci 119(6):3422. doi:10.1002/App.32992
16. Messori M, Bignotti F, De Santis R, Taurino R (2009) Polym Int 58(8):880. doi:10.1002/Pi.2606
17. Leclercq D, Bourget L, Corriu RJP, Mutin PH, Vioux A (1998) J Non-Cryst Solids 242(2–3):81
18. Niederberger M, Garnweitner G, Pinna N, Neri G (2005) Prog Solid State Chem 33(2–4):59. doi:10.1016/j.progsolidstchem.2005.11.032
19. Pinna N, Antonietti M, Niederberger M (2004) Colloid Surface A 250(1–3):211. doi:10.1016/j.colsurfa.2004.07.078
20. Pinna N, Neri G, Antonietti M, Niederberger M (2004) Angew Chem Int Ed 43(33):4345. doi:10.1002/anie.200460610
21. Pinna N, Niederberger M (2008) Angew Chem Int Ed 47(29):5292. doi:10.1002/Anie.200704541
22. Pinna N, Garnweitner G, Beato P, Niederberger M, Antonietti M (2005) Small 1(1):112. doi:10.1002/smll.200400014
23. Pinna N, Garnweitner G, Antonietti M, Niederberger M (2005) J Am Chem Soc 127(15):5608. doi:10.1021/ja042323r
24. Arnal P, Corriu RJP, Leclercq D, Mutin PH, Vioux A (1997) Chem Mater 9(3):694
25. Mutin PH, Vioux A (2009) Chem Mater 21(4):582. doi:10.1021/Cm802348c
26. Corriu R, Leclercq D, Lefevre P, Mutin PH, Vioux A (1992) Chem Mater 4(5):961
27. Corriu RJP, Leclercq D, Lefevre P, Mutin PH, Vioux A (1992) J Mater Chem 2(6):673
28. Corriu RJP, Leclercq D, Lefèvre P, Mutin PH, Vioux A (1992) J Non-Cryst Solids 146:301
29. Niederberger M, Bartl MH, Stucky GD (2002) Chem Mater 14(10):4364. doi:10.1021/cm021203k
30. Niederberger M, Garnweitner G, Krumeich F, Nesper R, Colfen H, Antonietti M (2004) Chem Mater 16(7):1202. doi:10.1021/cm031108r
31. Zhu J, Yang J, Bian ZF, Ren H, Liu YM, Cao Y, Li HX, He HY, Fan KN (2007) Appl Catal B 76(1–2):82. doi:10.1016/J.Apcatb.2007.05.017
32. Jia HM, Zheng Z, Zhao HX, Zhang LZ, Zou ZG (2009) Mater Res Bull 44(6):1312. doi:10.1016/j.materresbull.2008.12.016
33. Corradi AB, Bondioli F, Focher B, Ferrari AM, Grippo C, Mariani E, Villa C (2005) J Am Ceram Soc 88(9):2639
34. Morselli D, Bondioli F, Sangermano M, Messori M (2012) Polymer 53(2):283. doi:10.1016/j.polymer.2011.12.006
35. Morselli D, Messori M, Bondioli F (2011) J Mater Sci 46(20):6609. doi:10.1007/s10853-011-5610-9
36. Toby BH (2001) J Appl Crystallogr 34:210
37. Dreele ACLRBV (2004) General Structure Analysis System (GSAS). Los Alamos National Laboratory, Los Alamos
38. Brunauer S, Emmett PH, Teller E (1938) J Am Chem Soc 60(2):309
39. Kodera K (1962) In: Kubo K, Suito E, Nakagawa Y, Hayakawa S (eds) Powders (theory and applications). Maruzen, Tokyo
40. Messori M, Bondioli F, Dorigato A, Fabbri P, Pegoretti A (2008) Polym Eng Sci 48(3):448. doi:10.1002/pen.20973
41. Lide DR (2007) CRC handbook of chemistry and physics. CRC Press, Boca Raton
42. José Velasco M, Rubio F, Rubio J, Oteo JL (1999) Thermochim Acta 326 (1–2):91–97. doi:10.1016/s0040-6031(98)00580-2
43. Bondioli F, Darecchio ME, Luyt AS, Messori M (2011) J Appl Polym Sci 122(3):1792. doi:10.1002/App.34264